MNRAS **000**, 1-10 (2015) Preprint 28 June 2015 Compiled using MNRAS LaTeX style file v3.0

The Carnegie RR Lyrae Program: The Mid–Infrared RR Lyrae Period–Luminosity Relation in ω Cen

Meredith J. Durbin[1,2]★ Victoria Scowcroft[3] Wendy Freedman[4] Gurtina Besla[5] Giuseppe Bono[6,7] Maria–Rosa Cioni[8,9,10] Gisella Clementini[11] Kathryn Johnston[12] Nitya Kallivayalil[13] Juna Kollmeier[3] David Law[2] Barry Madore[3] Steve Majewski[13] Roeland van der Marel[2] Massimo Marengo[14] Andrew J. Monson[3] David Nidever[15] Grzegorz Pietrzynski[16,17] George Preston[3] Mark Seibert[3] Horace Smith[18] Igor Soszynski[16] Ian Thompson[3] Andrzej Udalski[16]

[1] *Pomona College, Claremont, CA 91711, USA*
[2] *Space Telescope Science Institute, 3700 San Martin Drive, Baltimore, MD 21218, USA*
[3] *Observatories of the Carnegie Institution of Washington, 813 Santa Barbara St., Pasadena, CA 91101, USA*
[4] *Department of Astronomy and Astrophysics, University of Chicago, 5640 S Ellis Ave, Chicago, IL 60637, USA*
[5] *Department of Astronomy and Steward Observatory, University of Arizona, 933 North Cherry Avenue, Tucson, AZ 85721, USA*
[6] *Univ. Roma "Tor Vergata", Via della Ricerca Scientifica, 1 - 00133, Roma, Italy*
[7] *INAF-OAR, via Frascati 33 - 00040, Monte Porzio Catone (RM), Italy*
[8] *Universtat Potsdam, Institut fur Physik und Astronomie, Karl-Liebknecht-Str. 24/25, 14476 Potsdam, Germany*
[9] *Leibniz-Institut fur Astrophysik Potsdam, An der Sternwarte 16, 14482 Potsdam, Germany*
[10] *University of Hertfordshire, Physics, Astronomy and Mathematics, College Lane, Hatfield AL10 9AB, United Kingdom*
[11] *INAF - Osservatorio Astronomico, Via Ranzani n. 1, 40127 Bologna, Italy*
[12] *Department of Astronomy, Columbia University, New York, NY 10027, USA*
[13] *Department of Astronomy, University of Virginia, Charlottesville, VA 22904-0818, USA*
[14] *Department of Physics and Astronomy, Iowa State University, Ames, IA, USA*
[15] *Department of Astronomy, University of Michigan, Ann Arbor, MI 48109, USA*
[16] *Warsaw University Observatory Al. Ujazdowskie 4, 00-478 Warszawa, Poland*
[17] *Departamento de Astronomia, Universidad de Concepcion, Casilla 160-C, Chile*
[18] *Department of Physics and Astronomy, Michigan State University, East Lansing, MI, USA 48824*

Accepted XXX. Received YYY; in original form ZZZ

ABSTRACT
Something something metallicity

Key words: keyword1 - keyword2 - keyword3

1 INTRODUCTION

The Carnegie Hubble Program (CHP) is a Warm *Spitzer* program with the aim of measuring H_0 to a systematic uncertainty of 3%, eventually reducing that uncertainty to 2% using *JWST*. The first part of the CHP used Cepheids as the primary distance indicator, using parallax measurements of Cepheids from *HST* (Benedict et al. 2007) to calibrate the zero–point of the Cepheid Period–Luminosity (PL) relation (also known as the Leavitt Law, or LL), leading out to Cepheid measurements in the Milky Way (MW, Monson et al. 2012) and Large Magellanic Cloud (LMC, Scowcroft et al. 2011). An initial recalibration of H_0 from CHP was presented in Freedman et al. (2012).

The CHP removed many systematics from the H_0 measurement by moving to the mid–infrared (extinction is reduced by a factor of 16 to 20, amplitude of Cepheid pulsation is reduced, intrinsic width of LL is reduced) and by using a single instrument (no effects from ground–to–space transformation, for example) but there are some effects that cannot be accounted for without further tests. By only using a single distance indicator (i.e. Cepheids) for the zero–point measurement, we have no understanding of the intrinsic accuracy of our measurement. With recent measurements from cosmic microwave background (CMB) experiments such as Planck (Planck Collaboration et al. 2015) in tension with local H_0 values, we must assess all possible sources of systematic uncertainty in our measurement. This is where the Carnegie RR Lyrae Program comes into play.

** VS NOTE: With regard to CMB - is measurements the

★ E-mail: mdurbin@stsci.edu

correct word here? Obviously Planck et al. make measurements, but they do not measure H_0, it is inferred from a model. What word would be more appropriate here? **

The Carnegie RR Lyrae Program (CRRP) assess a systematic that was unreachable in the original CHP – the intrinsic accuracy of the mid–infrared Cepheid standard candle distance scale when compared to the standard ruler distance scale of CMB and Baryon Acoustic Oscillation (BAO) measurements. With only one "test candle" it is impossible to make any assessment of this accuracy. However, when we have two standard candles with similar precision we can make meaningful comparisons and assess the systematic accuracy of both of them.

In the past RR Lyrae variables have often been thought of as the poor substitute for Cepheids in terms of distance scale measurements. They are intrinsically fainter, and in the optical follow a much shallower, even horizontal, PL relation. Determining an accurate distance to an RR Lyrae (RRL) in the V band requires knowledge of its [Fe/H] – a quantity which itself is not easy to obtain. However, in more recent years near– and mid–infrared observations have shown the true power of RRL as precision distance indicators. In a similar vein to Cepheids, HST parallaxes were obtained for several Galactic RRL calibrators Benedict et al. (2011) and several groups have been studying the populations of RRL in globular clusters and nearby dwarf spheroidal galaxies (NEED REFS).

In the mid–infrared RRL exhibit similar properties to Cepheids (Madore et al. 2013). Their light curve amplitudes are minimised as we are seeing deeper into the star. At the wavelengths observed by Warm *Spitzer* (3.6 and 4.5 μm) we do not see photospheric effects, but only the effects of temperature driving the pulsation. Essentially, the mid–infrared light curve is tracing the radius change of the star. A by–product of this effect is that the intrinsic width of the RRL PL relation is also minimised in the mid–infrared (mid–IR). The PL relation for pulsational variables can be thought of as a two–dimensional projection of the three–dimensional period–luminosity–colour relation (see figure 3 of Madore & Freedman (1991) for a graphical representation). As the colour–width decreases in the mid–IR, the width of the PL naturally decreases. As one moves from the optical to the mid–IR, the slope of the PL relation steepens and its dispersion dramatically decreases; this phenomenon has been demonstrated in simulations by Catelan et al. (2004), and by several observational efforts, as illustrated in fig. 4 of Madore et al. (2013). The slope should asymptotically approach the predicted slope of the period–radius relation, resulting in a slope between −2.4 and −2.8. Through this decrease in dispersion we have found that the intrinsic width of the mid–IR PL for RRL is in fact smaller than for Cepheids – 0.05 mag compared to 0.10 mag (Monson et al. 2015 [**I couldn't find this reference on the arxiv**], (Neeley et al. 2015)). This translates to an uncertainty on an individual RR Lyrae star of 2%, compared to 4% for Cepheids.

In this work we present the mid–IR PL relation for the RRL in the ω Cen Galactic Globular Cluster (GGC). Here we present a mid–infrared of the RR Lyrae period–luminosity (PL) relation in the IRAC channels 1 and 2 centred on 3.6 and 4.5 μm respectively, as well as a preliminary investigation into metallicity effects on the PL relation.

There are very few metallic or molecular transition lines in the mid–IR at typical RR Lyrae temperatures, so the effects of metallicity on luminosity should be minimised. However, ω Cen provides the ideal test bed for any effect that we may not have predicted. Such an effect is not out of the realm of possibility; for example, the CO band head at 4.5 μm has been found to have a significant dependence on metallicity, and has such prevented the IRAC 4.5 μm Cepheid observations from being used for distance measurements in the CHP. As our concern in this program is systematic precision, we must ensure that similar effects do not plague the RRL distance scale.

ω Cen in particular is ideal for calibrating the RR Lyrae period–luminosity–metallicity relation, as it contains 192 known RR Lyrae (Kaluzny et al. 2004) with a metallicity range spanning over 1.5 dex (Bono 2013, priv. comm.); a metallicity spread this wide is not found in any other GGC. As noted in Sollima et al. (2006a), one of the advantages of using globular clusters to calibrate PL coefficients is that all stars in a cluster can be considered to be at the same distance from Earth. We can therefore assume that any dispersion in the PL relation is a combination of the a) the intrinsic dispersion of the PL relation, b) the photometric uncertainties, and c) dispersion induced by the spread in metallicity of the RRL. We have measured the intrinsic dispersion of the RRL PL from other clusters (e.g. M4, Neeley et al. (2015)), and our photometric uncertainties are a well defined **constraint, value?? what is the correct word?**, so the only unknown in this problem is the dispersion due to the spread in metallicity of the cluster. We are lucky with ω Cen that we can also take a second approach to establishing the metallicity effect on the RRL PL relation. As it is such a unique object, ω Cen is extremely well studied and many of its RRL have spectroscopic or photometric metallicities available. As another test of the effect of metallicity, we use these measurements to assess the γ parameter for the GGC, where

$$\gamma = \frac{\Delta \mathrm{mag}}{[Fe/H]}, \tag{1}$$

similar to γ used to quantify the effect of metallicity on the zero–point of the Cepheid PL relation.

The paper is set out as follows: Section 2 details the observations and data reduction. Section 4 describes the mid–IR PL relations and Section 5 discusses the application of these to a distance measurement of ω Cen. Section 6 and Section 7 examine the effect of metallicity on mid–IR observations of RR Lyrae variables and its implications for distance measurements and the extragalactic distance scale. In Section 8 we present our conclusions.

2 OBSERVATIONS & DATA REDUCTION

The observations for this work were taken as part of the Warm *Spitzer* mission as part of the Carnegie RR Lyrae Program (PI W. Freedman, PID 90002). Three fields in ω Cen were chosen; their positions and the positions of known RR Lyrae are shown in Figure 1. To obtain optimal RRL light curves we observed each field twelve times over approximately 16 hours, roughly corresponding to the period of the longest period RRL we expected in the field. The observations of all three fields were taken on 2013-05-10 and 2013-05-11. Each field was observed using *Spitzer* IRAC (Fazio et al. 2004) with a 30s frame time with a medium scale, gaussian 5–point dither pattern to mitigate any image artefacts. Images were collected in both the 3.6 and 4.5 μm channels. The elongated field shapes (seen in Figure 1 come from the design of IRAC; while the [3.6] channel is collecting on–target data, the [4.5] channel collects off target data "for free", and vice versa. We chose to include these off–target fields to maximise the number of RRL in our final sample.

The science images were created using MOPEX (Makovoz et al. 2006), first running overlap correction on the corrected BCDs (cBCDs) then mosaicking them at 0.6 arcsec pixel scale using the drizzle algorithm. Mosaicked location–correction images were created at the same time.

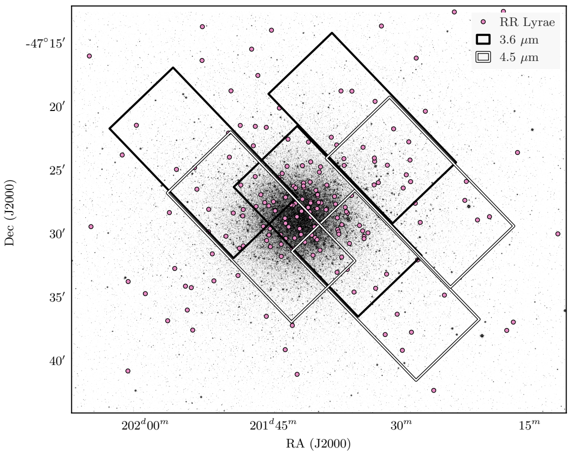

Figure 1. A K–band image of ω Cen from the FourStar camera, overlaid with the catalog of RR Lyrae (Kaluzny et al. 2004) and footprints of the three IRAC fields.

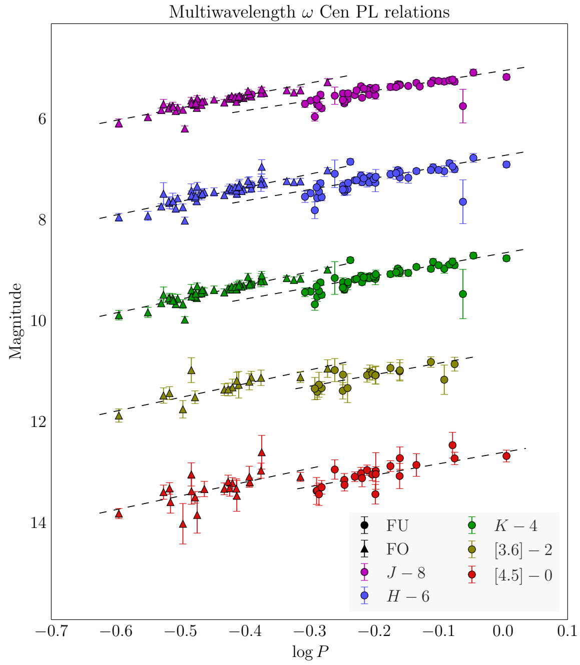

Figure 2. PL relations for JHK, 3.6 μm, and 4.5 μm photometry assuming an [Fe/H]= −1.584, corresponding to the average photometric metallicity from Rey et al. (2000). All uncrowded RRL for which we have photometry are included in these fits.

PSF photometry was performed using the DAOPHOT and ALLFRAME (Stetson 1987, 1994). The PSF model was created for each field/filter combination using the first epoch data. This was then applied to each other epoch. As the observations were taken so close together the effects of telescope rotation between epochs on the mosaicked PSF were minimal, so making a single good PSF model for each field/filter combination was much more efficient than creating one for every epoch.

Master star lists for ALLFRAME were created for each filter/field combination using a median mosaicked image created by MOPEX. We did not use a single master star list for both filters as only a small proportion (1/3) of the 3.6 μm and 4.5 μm fields overlap each other. Our photometry is calibrated to the standard system set by Reach et al. (2005).

The primary limiting factor in this data is crowding: 77 RR Lyrae variables out of the original catalog of 192 (Kaluzny et al. 2004) were rejected due to crowding. To decide which stars to reject we compared the *Spitzer* images to a K–band image from the FourStar infrared camera on Magellan (Persson et al. 2013), with a resolution of 0.159 arcsec. This enabled us to see which stars were significantly contaminated and adjust our final sample accordingly.

3 RESULTS

Our final photometry catalog, including magnitudes and errors for JHK, 3.6 μm, and 4.5 μm is presented in Table 8.

We calculate the average magnitude of each star by converting the individual time series magnitudes into fluxes, averaging those, and then converting the averaged flux back to a magnitude. The photometric errors of the time series data are added in quadrature to obtain the final error value.

Not really sure what else to put here; the photometry table is horrendously large and would be unwieldy anywhere other than an appendix. Also I don't know why TeX is referencing the table as table 8 when it's definitely not.

4 PERIOD–LUMINOSITY RELATIONS

For the final PL relations, we use only the stars for which we have photometry in all five bandpasses. While this introduced a marked sampling bias when it was done for Cepheids in the SMC (Scowcroft et al. 2015) due to uneven sampling of the full Cepheid distance range and instability strip width, we do not anticipate that these factors will be of concern for ω Cen RR Lyrae variables. ω Cen is an order of magnitude smaller in radius than the SMC, so the range of distances within the cluster relative to its distance from Earth is negligible for our purposes, and as previously mentioned, the intrinsic PL width of RR Lyrae variables in the mid–IR is half that of Cepheids (0.05 mag vs. 0.10 mag).

Our final RRL sample consists of 24 RRL (11 fundamental mode and 13 first overtone). We use the near– and mid–infrared PL relation parameters presented in **VS CHECK REF FOR BRAGA PAPER** as fiducial in all of our PL fitting. With the use of the theoretical PL relation coefficients, the distance modulus becomes the only free parameter in our fit. We fit all distance moduli using a weighted least–squares method.

Not all stars in our sample have known metallicity values, so we use an average [Fe/H] value for all RR Lyrae variables in the cluster. We use both photometric (Rey et al. 2000) and spectroscopic (Sollima et al. 2006b) metallicities for comparison. We find that there is little correspondence between individual metallicity measurements for stars which have both spectroscopic and photometric metallicity values, as shown in Figure 3, and that the average metallicities of the spectroscopic and photometric catalogs differ by nearly 0.1 dex. We use a mean photometric [Fe/H] of −1.584 and a spectroscopic [Fe/H] of −1.677.

The RRL PL relations for each adopted average metallicity are shown in Figures 5 and 4 and described in Table 4. The relations

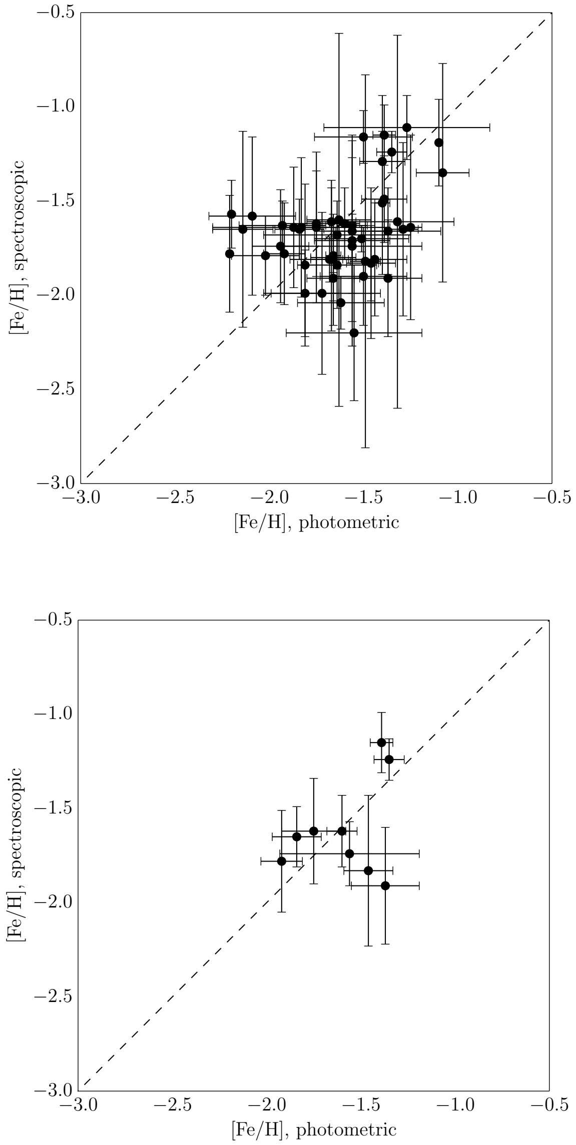

Figure 3. Spectroscopic vs. photometric measurements of [Fe/H] for RR Lyrae variables in ω Cen. Top: All stars for which both catalogs have [Fe/H] measurements. Bottom: only the stars which appear in our final sample.

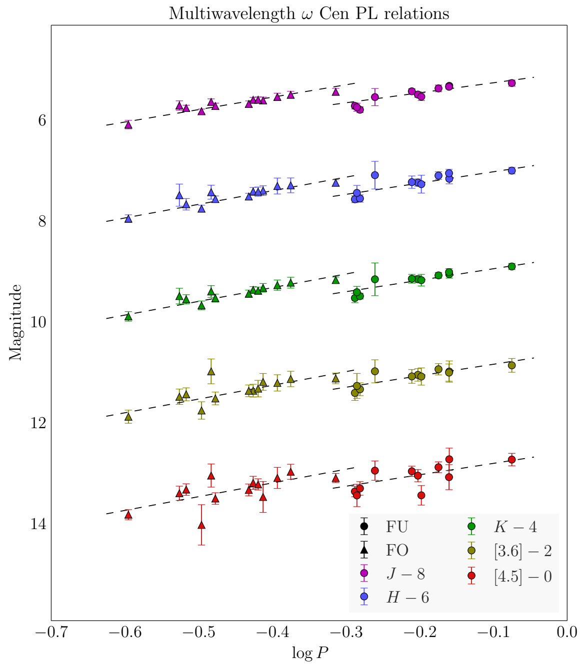

Figure 4. PL relations for JHK, 3.6 μm, and 4.5 μm photometry assuming an [Fe/H]= -1.584, corresponding to the average photometric metallicity from Rey et al. (2000). Only those RRL that appear in all five near– and mid–infrared bands are included in the fit.

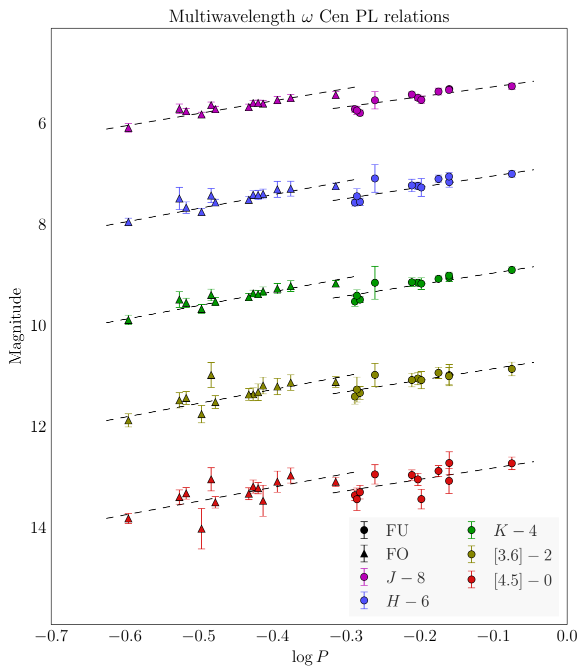

Figure 5. PL relations for JHK, 3.6 μm, and 4.5 μm photometry assuming an [Fe/H]= -1.677, corresponding to the average spectroscopic metallicity from Sollima et al. (2006b). Only those RRL that appear in all five near– and mid–infrared bands are included in the fit.

take the form

$$M = a + b \times \log P + c \times [Fe/H] \quad (2)$$

where a, b, and c are theoretically derived coefficients.

5 DISTANCE MODULI

We can combine the uncorrected distance moduli from each bandpass to obtain a mean reddening–corrected distance modulus. We fit the near–infrared reddening law from Cardelli et al. (1989) and mid–infrared law from Indebetouw et al. (2005) simultaneously, assuming the ratio of total to selective absorption $R_V = 3.1$. The resulting fits are shown in Figures 6 and 7.

Table 1. Mid–IR RR Lyrae period–luminosity relations for ω Cen.

Band	Mode	[Fe/H]	a	b	c	σ
[3.6]	FO	−1.584	−1.344	−2.718	0.152	0.021
	FO	−1.677	−1.344	−2.718	0.152	0.021
	FU	−1.584	−0.786	−2.276	0.184	0.035
	FU	−1.677	−0.786	−2.276	0.184	0.035
[4.5]	FO	−1.584	−1.348	−2.720	0.153	0.021
	FO	−1.677	−1.348	−2.720	0.153	0.021
	FU	−1.584	−0.775	−2.262	0.190	0.036
	FU	−1.677	−0.775	−2.262	0.190	0.036

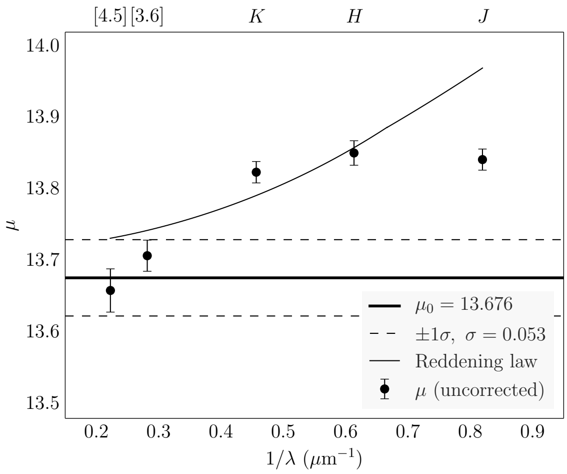

Figure 6. Distance moduli for *JHK*, 3.6 μm, and 4.5 μm photometry using the average photometric metallicity from Rey et al. (2000)

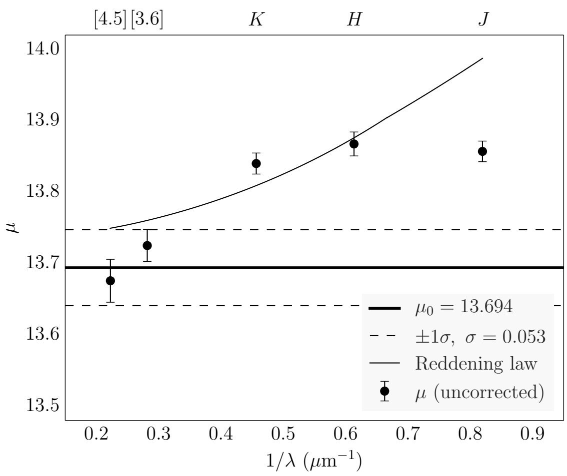

Figure 7. Distance moduli for *JHK*, 3.6 μm, and 4.5 μm photometry using the average spectroscopic metallicity from Sollima et al. (2006b)

Using photometric metallicities we obtain a mean reddening–corrected distance modulus of μ_0 = 13.678 ± 0.053, and with spectroscopic metallicities we obtain μ_0 = 13.694 ± 0.053. The difference between the two distance moduli is less than 0.02 mag, well within the ±0.053 mag errors. The fact that the two distance moduli are indistinguishable is the first indication that the infrared RRL PL relations are not sensitive to metallicity effects.

We average these distance moduli (thus essentially averaging the metallicities as well) to find a true mean distance modulus of μ_0 = 13.686 ± 0.053, which is in excellent agreement with prior measurements using near–infrared RR Lyrae period–luminosity relations (Del Principe et al. 2006) and and the eclipsing binary OGLEGC17 (Thompson et al. 2001), but significantly higher than the distances measured by dynamical modelling (van de Ven et al. 2006; Watkins et al. 2013)

6 METALLICITY

Theoretical models suggest that the metallicity dependence of the RR Lyrae PL relation should decrease monotonically from the optical to the near-infrared (Catelan et al. 2004; Bono et al. 2001), and observational evidence corroborates this; previous investigations performed on WISE data suggest no obvious metallicity dependence in the mid-IR PL relations (Madore et al. 2013). In the case of Cepheids, Scowcroft et al. (2011) and Scowcroft et al. (2015) have shown that in the 4.5 μm bandpass there is absorption due to a CO bandhead at 4.65 μm, which strengthens the metallicity dependence of the PL relation in this bandpass. However, this effect is due to the low temperature of Cepheid atmospheres and disappears in the hottest, shortest-period Cepheids, as the CO dissociates at temperatures above 6000 K (Monson et al. 2012). As even the coolest RRL have temperatures over 6000 K [**ref?**], we expect to see no such CO absorption in the 4.5 μm PL relation. However, there may be other unanticipated metallicity effects in the mid-IR PL relations. If there are any such effects, they must be smaller than the dispersion of the PL relations themselves.

If there is any correlation between [Fe/H] and the PL residuals, we expect it to be a linear one, consistent with the theoretical metallicity terms in the PL relation, $c \times [Fe/H]$. We fit a relation of the form

$$\Delta\mathrm{mag} = \gamma \times [Fe/H] + d \tag{3}$$

to the 3.6 μm and 4.5 μm PL residuals and metallicity values for stars with knowns individual metallicity values, as shown in Figures 8, 9, 10, and 11.

7 DISCUSSION

This section we can work on once you've worked on the others. I think it will write a lot of itself after you've done the other bits.

We find that although the scatter in the 3.6 μm and 4.5 μm PL relations is higher for ω Cen than it is for M4 (Neeley et al. 2015), there is no evidence that it is due to metallicity. When we examine [Fe/H] vs. $\Delta 3.6$ μm and $\Delta 4.5$ μm, γ is within 2σ of zero for all fits, indicating that there is no significant metallicity dependence in the PL residuals. When the outlier in [Fe/H] vs. 3.6 μm at [Fe/H] = −2.0 is removed from the photometric metallicities, the slopes of [Fe/H] vs. 3.6 μm and 4.5 μm both move within 1σ of zero.

Alternative explanations for the increased scatter relative to M4 include crowding and [other things here].

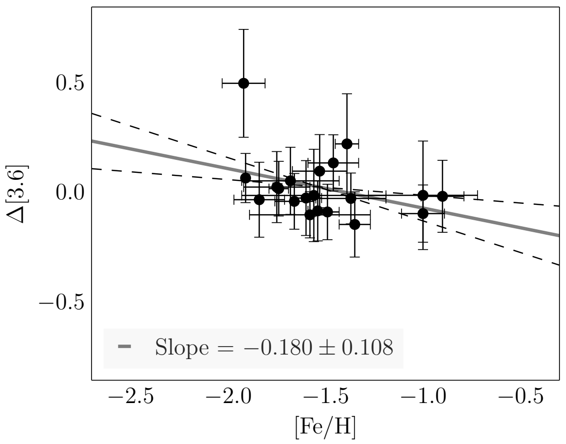

Figure 8. [Fe/H] vs. $\Delta 3.6$ μm using photometric metallicities

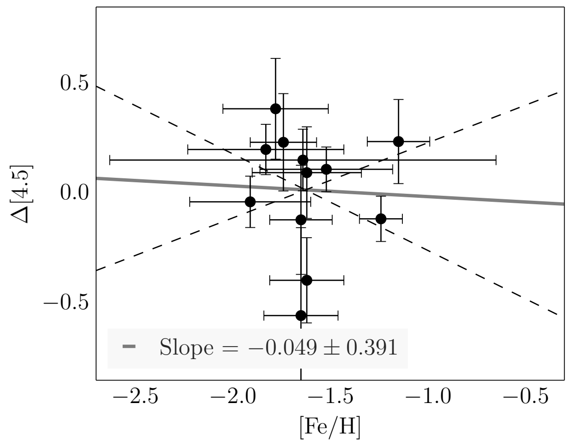

Figure 11. [Fe/H] vs. $\Delta 4.5$ μm using spectroscopic metallicities

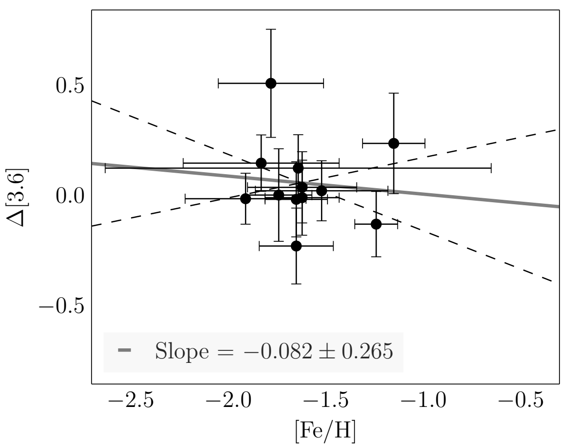

Figure 9. [Fe/H] vs. $\Delta 3.6$ μm using spectroscopic metallicities

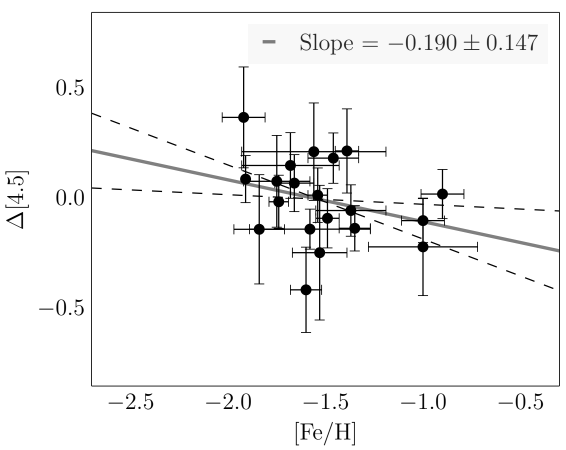

Figure 10. [Fe/H] vs. $\Delta 4.5$ μm using photometric metallicities

8 CONCLUSIONS

ACKNOWLEDGEMENTS

We thank Eric Persson for his many contributions to this project.

This work is based on observations made with the Spitzer Space Telescope, which is operated by the Jet Propulsion Laboratory, California Institute of Technology under a contract with NASA. Support for this work was provided by NASA through an award issued by JPL/Caltech.

REFERENCES

Benedict G. F., et al., 2007, AJ, 133, 1810
Benedict G. F., et al., 2011, AJ, 142, 187
Bono G., Caputo F., Castellani V., Marconi M., Storm J., 2001, MNRAS, 326, 1183
Cardelli J. A., Clayton G. C., Mathis J. S., 1989, ApJ, 345, 245
Catelan M., Pritzl B. J., Smith H. A., 2004, ApJS, 154, 633
Del Principe M., et al., 2006, ApJ, 652, 362
Fazio G. G., et al., 2004, ApJS, 154, 10
Freedman W. L., Madore B. F., Scowcroft V., Burns C., Monson A., Persson S. E., Seibert M., Rigby J., 2012, ApJ, 758, 24
Indebetouw R., et al., 2005, ApJ, 619, 931
Kaluzny J., Olech A., Thompson I. B., Pych W., Krzemiński W., Schwarzenberg-Czerny A., 2004, A&A, 424, 1101
Madore B. F., Freedman W. L., 1991, PASP, 103, 933
Madore B. F., et al., 2013, ApJ, 776, 135
Makovoz D., Roby T., Khan I., Booth H., 2006, in Society of Photo-Optical Instrumentation Engineers (SPIE) Conference Series. p. 0, doi:10.1117/12.672536
Monson A. J., Freedman W. L., Madore B. F., Persson S. E., Scowcroft V., Seibert M., Rigby J. R., 2012, ApJ, 759, 146
Neeley J. R., et al., 2015, preprint, (arXiv:1505.07858)
Persson S. E., et al., 2013, PASP, 125, 654
Planck Collaboration et al., 2015, preprint, (arXiv:1502.01589)
Reach W. T., et al., 2005, PASP, 117, 978
Rey S.-C., Lee Y.-W., Joo J.-M., Walker A., Baird S., 2000, AJ, 119, 1824
Scowcroft V., Freedman W. L., Madore B. F., Monson A. J., Persson S. E., Seibert M., Rigby J. R., Sturch L., 2011, ApJ, 743, 76
Scowcroft V., Freedman W. L., Madore B. F., Monson A., Persson S. E., Rich J., Seibert M., Rigby J. R., 2015, preprint, (arXiv:1502.06995)
Sollima A., Cacciari C., Valenti E., 2006a, MNRAS, 372, 1675

Sollima A., Borissova J., Catelan M., Smith H. A., Minniti D., Cacciari C., Ferraro F. R., 2006b, ApJ, 640, L43
Stetson P. B., 1987, PASP, 99, 191
Stetson P. B., 1994, PASP, 106, 250
Thompson I. B., Kaluzny J., Pych W., Burley G., Krzeminski W., Paczyński B., Persson S. E., Preston G. W., 2001, AJ, 121, 3089
Watkins L. L., van de Ven G., den Brok M., van den Bosch R. C. E., 2013, MNRAS, 436, 2598
van de Ven G., van den Bosch R. C. E., Verolme E. K., de Zeeuw P. T., 2006, A&A, 445, 513

Table 1. *JHK*, 3.6 μm, and 4.5 μm photometry

ID	RA (J2000)	Dec (J2000)	M_J	σ_J	M_H	σ_H	M_K	σ_K	$M_{[3.6]}$	$\sigma_{[3.6]}$	$M_{[4.5]}$	$\sigma_{[4.5]}$	P (days)	Mode	[Fe/H], p	$\sigma_{\text{[Fe/H], p}}$	[Fe/H], s	$\sigma_{\text{[Fe/H], s}}$
3	13:25:56.15	-47:25:53.8	13.247	0.06	12.982	0.064	12.882	0.06	12.841	0.137	12.708	0.124	0.841	0.0	-1.54	0.05	–	–
4	13:26:12.93	-47:24:18.8	13.475	0.055	13.219	0.073	13.133	0.069	13.03	0.124	13.026	0.121	0.627	0.0	-1.74	0.05	–	–
5	13:26:18.33	-47:23:12.4	13.7	0.059	13.549	0.068	13.507	0.092	13.387	0.148	13.34	0.103	0.515	0.0	-1.35	0.08	-1.24	0.11
7	13:27:00.90	-47:14:00.5	13.333	0.032	13.151	0.107	13.036	0.064	–	–	–	–	0.713	0.0	-1.46	0.08	–	–
8	13:27:48.45	-47:28:20.3	13.505	0.051	13.258	0.057	13.223	0.047	–	–	–	–	0.521	0.0	-1.91	0.28	–	–
9	13:25:59.58	-47:26:24.0	13.776	0.058	13.534	0.072	13.47	0.056	13.315	0.126	13.279	0.135	0.523	0.0	-1.49	0.06	–	–
10	13:26:06.99	-47:24:36.6	13.579	0.047	13.395	0.079	13.345	0.065	13.342	0.127	13.168	0.13	0.375	1.0	-1.66	0.10	–	–
11	13:26:30.59	-47:23:01.6	13.481	0.05	13.307	0.096	13.219	0.087	13.05	0.201	–	–	0.565	0.0	-1.67	0.13	-1.61	0.22
12	13:26:27.21	-47:24:06.2	13.59	0.064	13.379	0.097	13.305	0.086	13.168	0.167	13.448	0.306	0.387	1.0	-1.53	0.14	–	–
13	13:25:58.18	-47:25:21.6	13.353	0.067	13.081	0.077	13.058	0.058	12.918	0.112	12.86	0.107	0.669	0.0	-1.91	0.000	–	–
14	13:25:59.74	-47:39:09.6	13.588	0.038	13.343	0.068	13.365	0.056	–	–	13.299	0.156	0.377	1.0	-1.71	0.13	–	–
15	13:26:27.11	-47:24:38.0	13.245	0.062	13.02	0.106	12.954	0.087	13.149	0.29	–	–	0.811	0.0	-1.64	0.39	-1.68	0.18
16	13:27:37.69	-47:37:34.8	13.68	0.053	13.502	0.075	13.437	0.061	–	–	–	–	0.33	1.0	-1.29	0.08	-1.65	0.46
18	13:27:45.11	-47:24:56.6	13.371	0.035	13.131	0.083	13.1	0.057	13.006	0.148	–	–	0.622	0.0	-1.78	0.28	–	–
20	13:27:14.05	-47:28:06.3	13.41	0.051	13.21	0.123	13.125	0.087	13.06	0.137	12.94	0.102	0.616	0.0	–	–	-1.52	0.34
21	13:26:11.17	-47:25:58.8	13.578	0.057	13.399	0.092	13.361	0.071	13.301	0.164	13.2	0.112	0.381	1.0	-0.90	0.11	–	–
22	13:27:41.04	-47:34:07.6	13.572	0.042	13.38	0.056	13.288	0.058	–	–	–	–	0.396	1.0	-1.63	0.17	-1.60	0.99
23	13:26:46.50	-47:24:39.5	13.941	0.086	13.794	0.165	13.658	0.116	13.325	0.221	–	–	0.511	0.0	-1.08	0.14	-1.35	0.58
24	13:27:38.32	-47:34:14.5	13.419	0.042	13.218	0.047	13.138	0.048	–	–	–	–	0.462	1.0	-1.86	0.03	–	–
30	13:26:15.94	-47:29:56.0	13.521	0.074	13.287	0.158	13.251	0.103	13.188	0.162	13.071	0.209	0.404	1.0	-1.75	0.17	-1.62	0.28
32	13:27:03.32	-47:21:38.9	13.508	0.031	13.244	0.064	13.132	0.062	–	–	–	–	0.62	0.0	-1.53	0.16	–	–
33	13:25:51.60	-47:29:05.8	13.338	0.051	13.106	0.075	13.091	0.067	–	–	13.006	0.121	0.602	0.0	-2.09	0.23	-1.58	0.42
34	13:26:07.21	-47:33:10.4	13.273	0.047	13.018	0.049	12.916	0.044	–	–	12.838	0.224	0.734	0.0	-1.71	0.000	–	–
35	13:26:53.21	-47:22:34.7	13.586	0.04	13.463	0.082	13.356	0.08	–	–	–	–	0.387	1.0	-1.56	0.08	-1.63	0.36
36	13:27:10.11	-47:15:29.8	13.534	0.025	13.372	0.066	13.307	0.05	–	–	–	–	0.38	1.0	-1.49	0.23	–	–
38	13:27:03.30	-47:36:30.2	13.226	0.052	12.943	0.067	12.814	0.063	–	–	–	–	0.779	0.0	-1.75	0.18	-1.64	0.40
39	13:27:59.77	-47:34:42.3	13.56	0.031	13.415	0.049	13.308	0.047	–	–	–	–	0.393	1.0	-1.96	0.29	–	–
40	13:26:24.56	-47:30:46.2	13.517	0.076	13.25	0.177	13.153	0.115	13.062	0.171	13.416	0.194	0.634	0.0	-1.60	0.08	-1.62	0.19
44	13:26:22.39	-47:34:35.3	13.677	0.048	13.425	0.079	13.368	0.064	–	–	13.132	0.126	0.568	0.0	-1.40	0.12	-1.29	0.35
45	13:25:30.88	-47:27:21.0	13.513	0.051	13.201	0.052	13.164	0.049	–	–	13.07	0.096	0.589	0.0	-1.78	0.25	–	–
46	13:25:30.23	-47:25:51.8	13.299	0.056	12.998	0.057	12.947	0.049	–	–	–	–	0.687	0.0	-1.88	0.17	–	–
47	13:25:56.46	-47:24:12.0	13.42	0.068	13.223	0.062	13.15	0.061	13.099	0.105	13.073	0.091	0.485	1.0	-1.58	0.31	–	–
49	13:26:07.78	-47:37:55.5	13.566	0.04	13.238	0.067	13.22	0.056	–	–	13.099	0.171	0.605	0.0	-1.98	0.11	–	–
50	13:25:53.94	-47:27:35.8	13.647	0.05	13.402	0.052	13.362	0.049	–	–	13.305	0.193	0.386	1.0	-1.59	0.19	–	–
51	13:26:42.66	-47:24:21.4	13.597	0.05	13.378	0.113	13.27	0.099	13.315	0.287	–	–	0.574	0.0	-1.64	0.21	-1.84	0.23
54	13:26:23.54	-47:18:47.7	13.281	0.055	12.998	0.058	12.954	0.052	12.799	0.104	–	–	0.773	0.0	-1.66	0.12	-1.80	0.23
56	13:25:55.53	-47:37:44.1	13.643	0.033	13.386	0.075	13.353	0.06	–	–	13.232	0.12	0.568	0.0	-1.26	0.15	–	–
57	13:27:49.38	-47:36:50.5	13.234	0.051	12.995	0.063	12.882	0.05	–	–	–	–	0.794	0.0	-1.89	0.14	–	–
58	13:26:13.05	-47:24:03.0	13.66	0.06	13.495	0.062	13.421	0.071	13.345	0.116	13.309	0.117	0.37	1.0	-1.37	0.18	-1.91	0.31
59	13:26:18.43	-47:29:46.7	13.727	0.079	13.424	0.149	13.391	0.115	13.248	0.247	13.418	0.222	0.519	0.0	-1.00	0.28	–	–
63	13:25:07.96	-47:36:54.1	13.223	0.06	12.862	0.059	12.869	0.041	–	–	–	–	0.826	0.0	-1.73	0.09	–	–
64	13:26:02.22	-47:36:19.2	13.638	0.045	13.438	0.076	13.407	0.075	–	–	13.314	0.152	0.344	1.0	-1.46	0.23	–	–
66	13:26:33.08	-47:22:25.2	13.542	0.036	13.359	0.075	13.264	0.068	13.103	0.121	–	–	0.407	1.0	-1.68	0.34	–	–
67	13:26:28.62	-47:18:46.9	13.61	0.05	13.384	0.054	13.326	0.054	13.368	0.162	–	–	0.564	0.0	-1.10	0.000	-1.19	0.23
68	13:26:12.80	-47:19:35.7	13.258	0.072	13.004	0.053	12.97	0.05	12.928	0.174	–	–	0.535	1.0	-1.60	0.01	–	–
69	13:25:11.02	-47:37:33.5	–	–	–	–	13.112	0.047	–	–	–	–	0.635	0.0	-1.52	0.14	–	–
70	13:27:27.76	-47:33:42.7	13.529	0.045	13.282	0.102	13.254	0.077	–	–	–	–	0.391	1.0	-1.94	0.15	-1.74	0.30
72	13:27:33.11	-47:16:22.9	13.554	0.034	13.339	0.058	13.311	0.05	–	–	–	–	0.385	1.0	-1.32	0.22	–	–
73	13:25:53.75	-47:16:10.8	13.48	0.061	13.251	0.06	13.215	0.054	–	–	–	–	0.575	0.0	-1.50	0.09	–	–
74	13:27:07.22	-47:17:33.9	13.622	0.026	13.457	0.054	13.405	0.052	–	–	–	–	0.503	0.0	-1.83	0.36	–	–
75	13:27:19.70	-47:18:46.5	13.41	0.039	13.175	0.097	13.137	0.087	–	–	–	–	0.422	1.0	-1.49	0.08	-1.82	0.99
76	13:26:57.23	-47:20:07.7	13.634	0.041	13.488	0.06	13.449	0.068	–	–	–	–	0.338	1.0	-1.45	0.13	–	–
77	13:27:20.89	-47:22:05.6	13.474	0.046	13.264	0.098	13.199	0.073	–	–	–	–	0.426	1.0	-1.81	0.000	-1.84	0.43

Table 1 (cont'd)

ID	RA (J2000)	Dec (J2000)	M_J	σ_J	M_H	σ_H	M_K	σ_K	$M_{[3.6]}$	$\sigma_{[3.6]}$	$M_{[4.5]}$	$\sigma_{[4.5]}$	P (days)	Mode	[Fe/H], p	$\sigma_{[Fe/H]}$, p	[Fe/H], s	$\sigma_{[Fe/H]}$, s
79	13:28:24.99	-47:29:25.2	13.382	0.036	13.162	0.055	13.123	0.051	–	–	–	–	0.608	0.0	-1.39	0.18	–	–
81	13:27:36.68	-47:24:48.3	13.542	0.043	13.326	0.115	13.286	0.087	13.248	0.263	–	–	0.389	1.0	-1.72	0.31	-1.99	0.43
82	13:27:35.61	-47:26:30.3	13.579	0.055	13.324	0.083	13.296	0.062	–	–	13.827	0.359	0.336	1.0	-1.56	0.20	-1.71	0.56
83	13:27:08.42	-47:21:34.1	13.603	0.034	13.431	0.082	13.37	0.077	–	–	–	–	0.357	1.0	-1.30	0.22	–	–
84	13:24:47.45	-47:29:56.5	–	–	12.833	0.06	12.781	0.054	–	–	–	–	0.58	0.0	-1.47	0.10	–	–
85	13:25:06.49	-47:23:34.0	13.344	0.038	–	–	–	–	–	–	–	–	0.743	0.0	-1.87	0.31	–	–
94	13:25:57.06	-47:22:46.1	14.07	0.085	13.934	0.077	13.87	0.095	13.858	0.13	13.799	0.1	0.254	1.0	-1.00	0.11	–	–
95	13:25:24.95	-47:28:53.2	13.497	0.051	13.269	0.06	13.264	0.057	–	–	13.178	0.082	0.405	1.0	-1.84	0.55	–	–
97	13:27:08.49	-47:25:30.9	13.302	0.036	13.143	0.1	13.034	0.077	12.964	0.21	12.702	0.222	0.692	0.0	-1.56	0.37	-1.74	0.17
101	13:27:30.24	-47:29:51.0	13.708	0.057	13.484	0.105	13.436	0.079	–	–	–	–	0.341	1.0	-1.88	0.32	–	–
102	13:27:22.11	-47:30:12.3	13.32	0.041	13.033	0.076	12.993	0.069	12.984	0.171	13.056	0.249	0.691	0.0	-1.84	0.13	-1.65	0.16
103	13:27:14.29	-47:28:36.3	13.62	0.061	13.409	0.139	13.377	0.116	12.96	0.246	13.024	0.229	0.329	1.0	-1.92	0.11	-1.78	0.27
104	13:28:07.76	-47:33:44.9	13.732	0.333	13.626	0.434	13.452	0.487	–	–	–	–	0.867	0.0	-1.83	0.18	–	–
105	13:27:46.02	-47:32:43.9	13.768	0.05	13.615	0.07	13.533	0.062	–	–	–	–	0.335	1.0	-1.24	0.18	–	–
107	13:27:14.05	-47:30:57.9	13.597	0.059	13.34	0.131	13.301	0.104	–	–	13.351	0.265	0.514	0.0	-1.36	0.11	–	–
115	13:26:12.30	-47:34:17.5	13.401	0.042	13.176	0.06	13.103	0.044	–	–	16.427	0.348	0.63	0.0	-1.87	0.01	-1.64	0.32
117	13:26:19.91	-47:29:21.0	13.48	0.069	13.274	0.147	13.202	0.107	13.11	0.153	12.949	0.149	0.422	1.0	-1.68	0.25	–	–
120	13:26:25.52	-47:32:48.6	13.525	0.171	13.072	0.273	13.135	0.325	12.958	0.228	12.927	0.191	0.549	0.0	-1.39	0.06	-1.15	0.16
121	13:26:28.17	-47:31:50.5	13.741	0.055	13.648	0.113	13.531	0.091	13.414	0.128	13.302	0.115	0.304	1.0	-1.46	0.13	-1.83	0.40
122	13:26:30.31	-47:33:02.2	13.369	0.061	13.132	0.146	13.062	0.084	13.057	0.179	13.019	0.148	0.635	0.0	-2.02	0.18	-1.79	0.21
123	13:26:51.17	-47:37:13.2	13.462	0.054	13.239	0.064	13.174	0.06	–	–	–	–	0.474	1.0	-1.64	0.01	–	–
124	13:26:54.49	-47:39:07.5	13.708	0.046	13.51	0.062	13.482	0.081	–	–	–	–	0.332	1.0	-1.33	0.23	–	–
125	13:26:48.92	-47:41:03.7	13.42	0.053	13.2	0.055	13.153	0.052	–	–	–	–	0.593	0.0	-1.67	0.22	-1.81	0.38
126	13:28:08.03	-47:40:46.7	13.642	0.038	13.467	0.058	13.37	0.054	–	–	–	–	0.342	1.0	-1.31	0.13	–	–
127	13:25:19.36	-47:28:37.6	–	–	–	–	13.579	0.061	–	–	13.573	0.217	0.305	1.0	-1.59	0.08	–	–
128	13:26:17.75	-47:30:13.0	13.207	0.062	12.927	0.109	12.81	0.068	–	–	12.445	0.256	0.835	0.0	-1.88	0.04	–	–
130	13:26:09.93	-47:13:40.0	13.688	0.072	13.527	0.111	13.418	0.086	–	–	–	–	0.493	0.0	-1.46	0.17	–	–
147	13:27:15.86	-47:31:09.2	13.397	0.043	12.934	0.142	13.083	0.078	–	–	12.585	0.333	0.423	1.0	-1.66	0.14	–	–
149	13:27:32.94	-47:13:43.6	13.354	0.053	13.061	0.12	13.024	0.083	–	–	–	–	0.683	0.0	-1.21	0.24	–	–
150	13:27:40.21	-47:36:00.1	13.068	0.067	12.757	0.086	12.692	0.062	–	–	–	–	0.899	0.0	-1.76	0.34	–	–
151	13:28:25.40	-47:16:00.2	13.501	0.046	13.301	0.071	13.265	0.056	–	–	–	–	0.408	0.0	-1.30	0.24	–	–
163	13:25:49.42	-47:20:21.5	13.763	0.064	13.557	0.055	13.545	0.087	–	–	–	–	0.313	1.0	-1.18	0.27	–	–
168	13:25:52.78	-47:32:02.9	14.176	0.052	14.0	0.07	13.96	0.062	–	–	–	–	0.321	1.0	–	–	–	–
169	13:27:20.47	-47:23:59.1	13.805	0.044	13.735	0.067	13.652	0.087	13.734	0.172	14.001	0.401	0.319	1.0	–	–	-1.65	0.19
184	13:27:28.50	-47:31:35.4	13.778	0.041	13.624	0.095	13.536	0.067	–	–	–	–	0.303	1.0	–	–	–	–
185	13:26:04.13	-47:21:45.0	13.701	0.057	13.545	0.062	13.508	0.079	13.496	0.126	13.479	0.115	0.333	1.0	–	–	–	–
261	13:27:15.41	-47:21:29.5	13.431	0.031	13.212	0.064	13.113	0.068	–	–	–	–	0.403	1.0	–	–	-1.50	0.35
263	13:26:13.13	-47:26:09.7	13.155	0.057	12.888	0.059	12.746	0.055	–	–	12.66	0.117	1.012	0.0	–	–	-1.73	0.19
274	13:26:43.73	-47:22:48.2	13.828	0.037	13.758	0.079	13.65	0.077	–	–	–	–	0.311	1.0	–	–	–	–
276	13:27:16.51	-47:33:17.6	13.727	0.072	13.614	0.159	13.533	0.084	–	–	–	–	0.308	1.0	–	–	–	–
280	13:27:09.33	-47:23:05.7	13.951	0.041	13.905	0.09	13.816	0.101	–	–	–	–	0.282	1.0	–	–	–	–
285	13:25:40.20	-47:34:48.4	13.687	0.059	13.504	0.093	13.503	0.052	–	–	13.358	0.256	0.329	1.0	–	–	–	–
288	13:28:10.32	-47:23:47.8	13.809	0.038	13.719	0.054	13.635	0.067	–	–	–	–	0.295	1.0	–	–	–	–
289	13:28:03.68	-47:21:27.9	13.743	0.046	13.618	0.052	13.584	0.075	–	–	–	–	0.308	1.0	–	–	–	–
291	13:26:38.52	-47:33:28.0	13.674	0.064	13.518	0.154	13.444	0.091	–	–	–	–	0.334	1.0	–	–	–	–
357	13:26:17.77	-47:30:23.4	13.692	0.094	13.468	0.22	13.468	0.155	13.462	0.152	13.375	0.14	0.298	1.0	–	–	-1.64	0.99

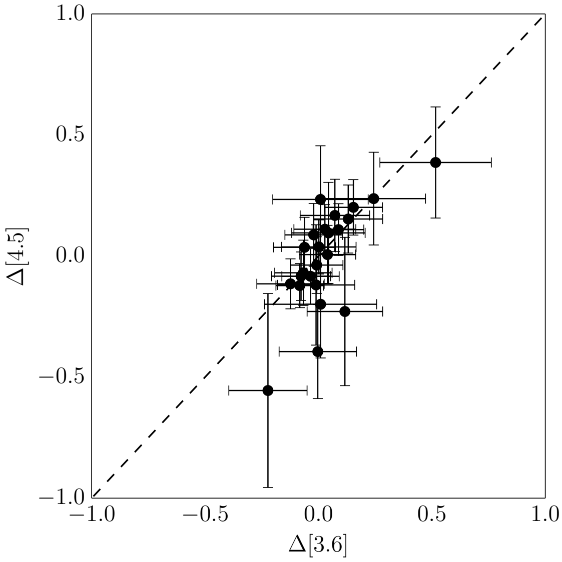

Figure 1. Δ3.6 μm vs. Δ4.5 μm using spectroscopic metallicities

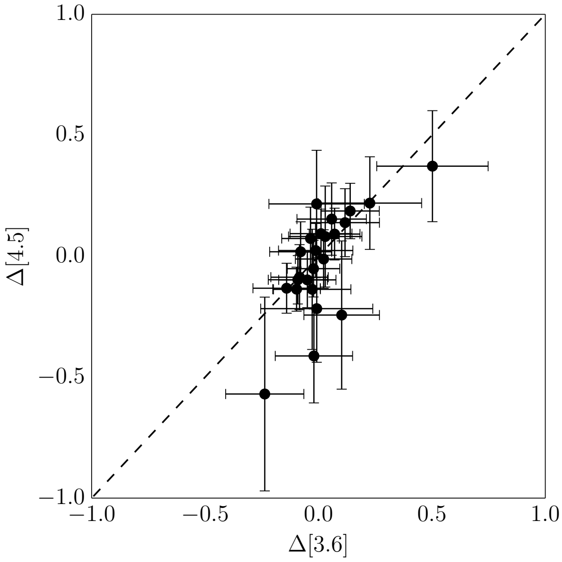

Figure 2. Δ3.6 μm vs. Δ4.5 μm using photometric metallicities

This paper has been typeset from a TEX/LATEX file prepared by the author.